Effective interactions and nuclear structure using 180 MeV protons. II. ^{28}Si(p,p')

Q. Chen,[a] J. J. Kelly,[b] P. P. Singh,[a] M. C. Radhakrishna,[a] W. P. Jones,[a] and H. Nann[a]

[a]*Department of Physics, Indiana University, Bloomington, Indiana 47401*
[b]*Department of Physics, University of Maryland, College Park, Maryland 20742*
(Received 27 November 1989)

Differential cross sections and analyzing powers for the scattering of 180 MeV protons have been measured for 14 states of ^{28}Si for momentum transfers between about 0.4 and 2.1 fm^{-1}. Medium modifications to the effective interaction for normal-parity isoscalar transitions were studied using transition densities fitted to electroexcitation data to minimize uncertainties due to nuclear structure. An empirical effective interaction, guided by nuclear matter theory, was fitted to inelastic scattering data for five states of ^{28}Si using self-consistent distorted waves. A good fit to the inelastic scattering data was achieved with an interaction similar to previous results for ^{16}O. The elastic data, which were not fitted, are also described well. In addition, we tested for mass dependence in the empirical effective interaction by repeating the analysis using data for both ^{16}O and ^{28}Si simultaneously. This global analysis produced an interaction intermediate between the two independent results without compromising the fit to either data set. Therefore, the effective interaction in finite nuclei appears to depend strongly upon local density but only weakly upon target.

I. INTRODUCTION

In this paper, the second in a series of three papers discussing proton scattering data at 180 MeV, we use new data for ^{28}Si to investigate the possibility that medium modifications to the two-nucleon effective interaction may depend upon the mass of the target. Previously,[1] using 180 MeV proton scattering data for ^{16}O, we found that the effective interaction depends strongly upon the local density in the interaction region and that the Paris-Hamburg (PH) interaction[2] provides the best available theoretical description of normal-parity isoscalar transitions. However, residual discrepancies between calculations and data indicated that substantially larger modifications of the effective interaction are required at low density than are predicted by the local density approximation (LDA). These effects were then investigated by fitting an empirical effective interaction to the ^{16}O inelastic scattering data using the methods developed in Ref. 3. Our results suggested that Pauli blocking in finite nuclei is more effective at low density and less effective at high density than for infinite nuclear matter of corresponding density.

In spite of the failure of the empirical effective interaction to heal to the free interaction at zero density, the LDA successfully described all of the data for a single target. A more stringent test of the concept of local nuclear matter density can be made by fitting the density dependence of the effective interaction to data for another target independently. If the LDA is sound, the same interaction should emerge, including the suppression at zero density.

We have measured cross sections and analyzing powers for the scattering of 180 MeV protons by ^{28}Si for momentum transfers between about 0.4 and 2.1 fm^{-1}. Five normal-parity transitions for which reasonably accurate

transition densities could be extracted from the available electron scattering data were used to analyze the two-nucleon effective interaction. The transition densities for the 0_2^+ and 2_3^+ states have enough interior strength to sample the density dependence of the effective interaction. The 2_1^+, 4_1^+, and 5_1^- transition densities are more surface peaked, so that these transitions are sensitive to changes in the effective interaction for low density.

When medium modifications to the effective interaction are fitted to the data for ^{28}Si alone, we obtain a good fit with an interaction qualitatively similar to, but quantitatively different from, the interaction fitted to ^{16}O data alone. When both sets of data are fitted simultaneously, the fitted interaction is intermediate between the two independent analyses yet still provides equally good fits to both data sets. Therefore, the data are compatible with an effective interaction which depends strongly upon local density but which is independent of target.

The experiment is described in Sec. II. Our analysis of the available electron scattering data for normal-parity states of ^{28}Si is presented in Sec. III. The proton scattering data are interpreted in Sec. IV and our conclusions are summarized in Sec. V.

II. EXPERIMENT

The experiment was performed using 180-MeV protons at the Indiana University Cyclotron Facility. Scattered protons were analyzed by the QDDM spectrometer and detected with a standard focal-plane array consisting of a helical wire chamber and two plastic scintillators. The target was a self-supporting natural ^{28}Si foil with thickness 15.7 mg/cm^2 that was also used by Refs. 4 and 5. Our elastic cross sections agree with those of Ref. 4 within about ±4%.

The beam polarization was measured every eight hours using the low-energy ^{4}He polarimeter located after the injector cyclotron. Average polarizations of 0.773 ± 0.008 for spin-up and 0.783 ± 0.013 for spin-down were obtained with little variation between measurements.

The experimental resolution varied between about 70 and 100 keV FWHM. A typical spectrum, with about 100 keV resolution FWHM, is shown in Fig. 1. The spectrum was fitted using the ALLFIT program described in Refs. 6 and 7. Known positions[8] for several strong peaks were used to calibrate the kinematic scale. The separations between closely spaced levels were constrained to accurately known values. It was then possible to obtain reliable results even when the spacing was somewhat less than the experimental resolution. Most notably we were able to separate the 2_2^+ and 2_3^+ peaks at 7.381 and 7.417 MeV. Further details of the experiment and data analysis may be found in Ref. 9.

Data tables are on deposit with the Physics Auxiliary Publication Service (PAPS).[10] Normal-parity data include elastic scattering and the 0_2^+ (4.979 MeV), 1_1^- (8.904 MeV), 2_1^+ (1.779 MeV), 2_2^+ (7.381 MeV), 2_3^+ (7.417 MeV), 2_4^+ (7.933 MeV), 2_5^+ (8.259 MeV), 4_1^+ (4.617 MeV), and 5_1^- (9.702 MeV) states. The 3_1^- and 4_2^+ states at 6.879 and 6.889 MeV could not be separated and are reported as a doublet. In addition, data for several abnormal-parity transitions are tabulated but are not discussed further here. These include the 3_2^+ (7.799 MeV) and 4_1^- (8.413 MeV) states. The data were collected for center-of-mass scattering angles between about 6° and 42°. One additional measurement was also made at 62°.

III. ELECTRON SCATTERING

Unambiguous interpretation of nucleon scattering data requires more accurate knowledge of transition densities than can be provided by any available theory of nuclear structure. Hence, we rely upon electron scattering data for this information. However, published transition densities are available for only a few of the states of interest. Therefore, we have analyzed the available electron scattering data for these states.

In plane-wave approximation, the electroexcitation cross section for a $J_i \rightarrow J_f$ transition becomes[11]

$$\frac{d\sigma}{d\Omega} = \eta\sigma_{\text{Mott}}Z^2 \sum_J [V_L(\theta)|F_J^L(q)|^2 + V_T(\theta)|F_J^T(q)|^2] ,$$

$$(1)$$

where F_J^L and F_J^T are longitudinal and transverse form factors for multipole J. The Mott cross section σ_{Mott}, recoil factor η, and angular factors V_L and V_T are simple kinematic factors that may be found in standard references.[11] It is convenient to parametrize the form factors by[12]

$$F_J^L(z) = \frac{\sqrt{4\pi}}{Z}\frac{q^J}{(2J+1)!!}f(q)e^{-y}\sum_\nu A_\nu y^\nu , \qquad (2a)$$

$$F_J^T(q) = \frac{\sqrt{4\pi}}{Z}\left[\frac{J+1}{J}\right]^{1/2}\frac{\omega}{q}\frac{q^J}{(2J+1)!!}f(q)e^{-y}\sum_\nu B_\nu y^\nu , \qquad (2b)$$
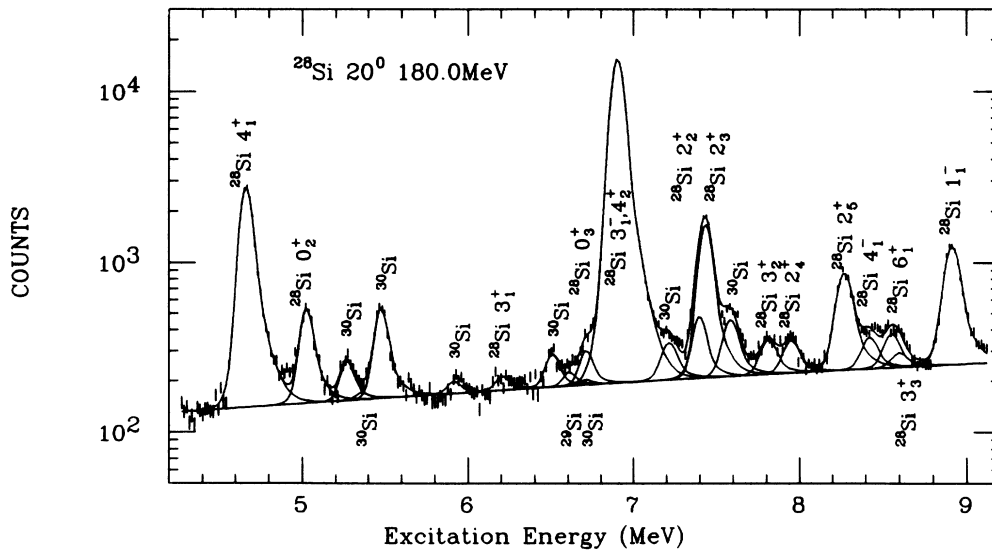
FIG. 1. Sample fitted spectrum for the 4–9-MeV excitation region for the scattering of 180 MeV protons by a natural silicon target.

where $y = (qb/2)^2$ and where b is an appropriate oscillator parameter. The optional form factor $f(q)$ can include nucleon and/or center-of-mass form factors, depending upon the interpretation of the expansion coefficients A_ν and B_ν. This parametrization makes the long-wavelength limit explicit and is consistent with the continuity equation if we require $A_0 = B_0$. The longitudinal and transverse contributions were separated by fitting these parametrizations to all available electron scattering data for each state. However, no significant transverse contributions to the transitions of interest could be found.

In addition, the low-q form factor can be constrained by lifetime data. At the photon point $q = \omega$, the transverse form factor is related to the partial width $\Gamma(J_f \rightarrow J_i)$ by

$$|F_J^T(\omega)|^2 = \frac{2J_f + 1}{2J_i + 1} \frac{\Gamma(J_f \rightarrow J_i)}{2Z^2 \alpha \omega} , \tag{3}$$

where α is the fine structure constant, J_i is the ground-state spin, and J_f is the spin of the state with excitation energy ω. The lifetime and branching ratio data compiled by Endt[13] for the 1^- and 2^+ states have been included in the analysis.

The longitudinal form factor is related to the transition charge density ρ_J^{ch} by the Fourier-Bessel transform

$$F_J^L(q) = \frac{\sqrt{4\pi}}{Z} \frac{\hat{J}_f}{\hat{J}_i} \tilde{\rho}_J^{ch}(q) , \tag{4a}$$

$$\tilde{\rho}_J(q) = \int dr \, r^2 j_J(qr) \rho_J(r) , \tag{4b}$$

where J is the multipolarity and $\hat{x} = \sqrt{2x + 1}$. Assuming that the neutron and proton densities are equal for isoscalar transitions, the point-proton density $\tilde{\rho}_J$ is related to the charge density by

$$\tilde{\rho}_J^{ch}(q) = \tilde{\rho}_J(q) f(q) , \tag{5}$$

where $f(q) = [1 + (q/\Lambda)^2]^{-2}$ with $\Lambda = 4.33$ fm^{-1}. Using the fitted form factor, we then expressed the point-proton density in the Laguerre-Gaussian expansion (LGE)

$$\rho_J(r) = x^J e^{-x^2} \sum_n C_n L_n^{J+1/2}(2x^2) , \tag{6}$$

where $x = r/b$ and where $L_n^a(z)$ is a generalized Laguerre polynomial. The A and C coefficients are related by

$$\left[\frac{\hat{J}_f}{\hat{J}_i} (2J + 1)!! \frac{\sqrt{\pi}}{4} b^3 \left[\frac{b}{2} \right]^J \right] C_n$$
$$= \sum_{m=n}^{N} A_m \frac{m!}{(m-n)!} 2^{n-2m} \frac{(2J + 2m + 1)!!}{(2J + 2n + 1)!!} . \tag{7}$$

A common oscillator parameter $b = 1.835$ fm was used for all states.

Finally, it is often useful to describe the strength and shape of the transition density by the moments

$$M_{\lambda J} = \int dr \, r^{2+\lambda} \rho_J(r) . \tag{8}$$

Note that we define $M_{\lambda J}$ in terms of the point distribution ρ_J rather than the charge distribution ρ_J^{ch}. For transitions allowed when $q \rightarrow 0$, the matrix element M_p and transition radius R_p are traditionally defined as

$$M_p = M_{JJ}, \quad R_p^2 = \frac{M_{J+2,J}}{M_{JJ}} \quad \text{(allowed)} . \tag{9}$$

For forbidden or almost forbidden transitions, the moment M_{JJ} vanishes or is very small. It is then more useful to define

$$M_p = M_{J+2,J}, \quad R_p^2 = \frac{M_{J+4,J}}{M_{J+2,J}} \quad \text{(forbidden)} , \tag{10}$$

for $0^+ \rightarrow 0^+$ or $0^+ T = 0 \rightarrow 1^- T = 0$ transitions. The sign of M_p cannot be determined from cross-section data and is thus arbitrarily taken as positive. Occasionally we find that densities with more than one major lobe have negative values of R_p^2. Therefore, we customarily assign the sign of R_p^2 to R_p.

Except for the 2_1^+ and 4_1^+ states, the range of momentum transfer for which data are available is too limited for "model independent" analysis. Therefore, we analyzed the data in plane-wave approximation, with the effective momentum transfer,[11] using only as many terms from the expansions in q^2 as could be determined unambiguously. However, although this procedure makes optimal use of the limited available data, it does not yield realistic uncertainties for the transition density or its moments. Hence, these uncertainties are omitted from the

TABLE I. Transition density parameters fitted to ^{28}Si(e,e') data. LGE coefficients C_n are in units of 10^{-2} fm^{-3}.

State	ω (MeV)	χ_ν^2	C_0	C_1	C_2	C_3	M_p[a]	R_p (fm)	References
0_2^+	4.98	1.0	1.750	-3.904	-2.767	1.105	2.171	5.574	14,15
1_1^-	8.90	1.2	1.907	-1.969	-1.545		4.322	5.864	16
2_1^+	1.78	6.2	7.676	-4.605	0.054	0.182	7.465	3.823	14,15,17–19
2_2^+	7.38	0.6	-0.743	-1.142			1.124	4.479	15
2_3^+	7.42	0.3	3.643	-0.146	-0.179		0.949	2.476	15
2_4^+	7.93	0.6	0.030	-0.460	0.272		1.309	4.720	15
2_5^+	8.26	0.4	1.886	-0.552	-0.366		0.288	-4.466	15
4_1^+	4.62	1.9	2.031	-0.231	-0.025		52.29	4.405	14,15,19
5_1^-	9.70	1.1	0.957	-0.091			286.7	4.946	16

[a]The units of M_p are e^2 fm^{L+2} for $L > 1$ or e^2 fm^{L+4} for $L \leq 1$.
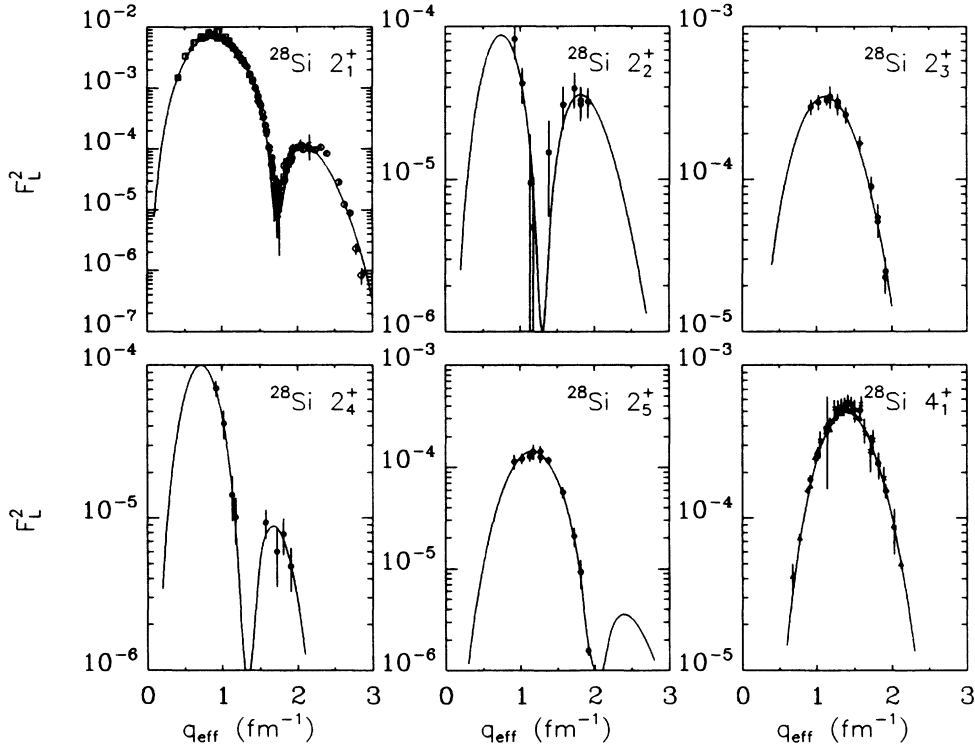
FIG. 2. Longitudinal form factors for 2^+ and 4^+ states of ^{28}Si. Data from Ref. 13 are shown as crosses, Refs. 15 and 16 as solid circles, Ref. 17 as open circles, Ref. 18 as squares, and Ref. 19 as triangles. The solid curves portray plane-wave fits.

tabulated results. In addition, we have performed more complete distorted-wave analyses for the 2_1^+ and 4_1^+ states. We find that the effects of distortion upon the fitted densities are too small to affect the later analysis of the (p,p') data.

The results of our analysis of the lifetime and electroexcitation data reported by Refs. 13–19 are summarized in Table I. Fitted form factors are displayed in Figs. 2–4. In these figures, data for $\theta < 140°$ are shown as
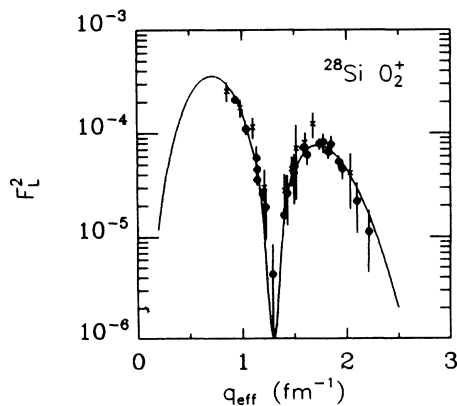
FIG. 3. Fitted form factor for the 0_2^+ state of ^{28}Si based upon the data of Ref. 14 (crosses) and Ref. 15 (solid circles).
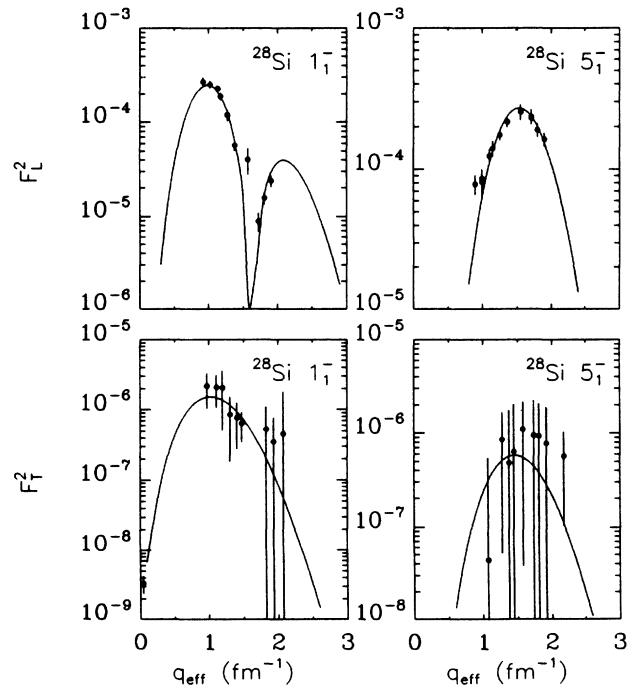
FIG. 4. Separated form factors for the 1_1^- and 5_1^- states of ^{28}Si are compared with data from Ref. 16.

longitudinal form factors after subtraction of the fitted transverse form factors. Similarly, data for $\theta > 140°$ are shown as separated transverse form factors. Uncertainties in the subtracted quantities are added in quadrature to the plotted error bars. The transverse form factors were found to be negligibly small for all of the positive-parity states and only on the order of 1% of the longitudinal form factors even for the negative-parity states.

The data available for the 2_1^+, 2_3^+, 4_1^+, and 5_1^- states are sufficient to determine the longitudinal form factor, and hence proton density, with relatively little uncertainty. Data for the 0_2^+ state are lacking at and below the first peak of the form factor, but the higher-q data appear to be sufficiently precise to yield a reliable fit anyway. The absence of low-q data for the 2_2^+ and 2_4^+ states is more serious and disqualifies these states from the fit to be made for the proton scattering data. We found that the 2_5^+ data could not be fitted well with less than three terms of the LGE expansion when the oscillator parameter $b = 1.835$ fm is held constant. Although the resulting fit is good for $q < 2$ fm^{-1}, a substantial second maximum for which there is no data emerges. The negative transition radius for the 2_5^+ state reveals a rather peculiar transition density.

Finally, the ground-state density was obtained by unfolding the nucleon form factor from the model-independent charge density tabulated by Ref. 20. This density was also used to calculate elastic scattering so that 2_1^+ form factor data could be obtained from the relative measurements of Brain et al.[18]

IV. RESULTS

A. Empirical effective interaction for ^{28}Si

Calculations for proton scattering were performed using the same methods and notation as described in Refs. 3 and 6. For the analysis of the empirical effective interaction we select the 0_2^+, 2_1^+, 2_3^+, 4_1^+ and 5_1^- states of ^{28}Si. Additional 5_1^- data extending to about 2.8 fm^{-1} are available from Olmer et al;[5] these data are included on the figures but are omitted from the analysis because our knowledge of the 5_1^- form factor is limited to $q \lesssim 2$ fm^{-1}. We have selected the states for which the available (e, e') data appear to define the transition densities with the least ambiguity. These densities are plotted in Fig. 5. The 0_2^+ and 2_3^+ states have substantial interior densities and provide good sensitivity to the high-density properties of the effective interaction. The other states are more surface peaked in character and are primarily sensitive to the low-density interaction.

Inelastic scattering calculations based upon the Paris-Hamburg (PH) effective interaction are compared with the data in Figs. 6 and 7. The dashed curves portray the local density approximation (LDA), whereas the dotted curves represent impulse approximation (IA) results obtained by neglecting the density dependence of the PH interaction for the transition potentials. Both of these sets of calculations employ LDA optical potentials computed from the PH interaction. Elastic scattering calculations for the LDA and IA are compared in Fig. 8 with the
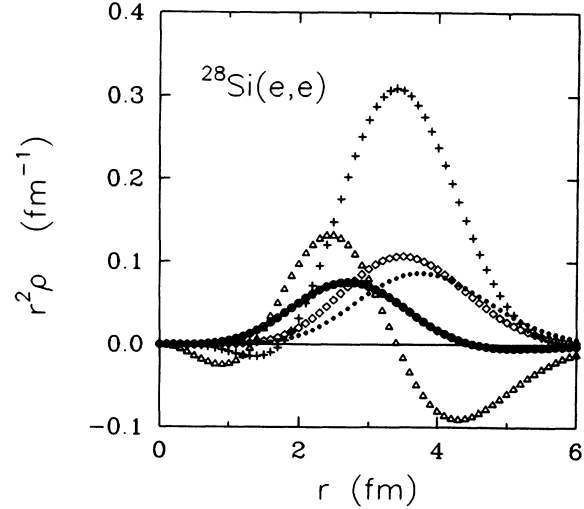
FIG. 5. Selected transition densities fitted to ^{28}Si(e, e') data. Triangles describe the 0_2^+ state, pluses the 2_1^+ state, solid circles the 2_3^+ state, diamonds the 4_1^+ state, and open circles the 5_1^- state. Notice that the 0_2^+ density has a strong interior lobe and that the 2_3^+ density peaks well inside the 2_1^+, 4_1^+, and 5_1^- surface densities.
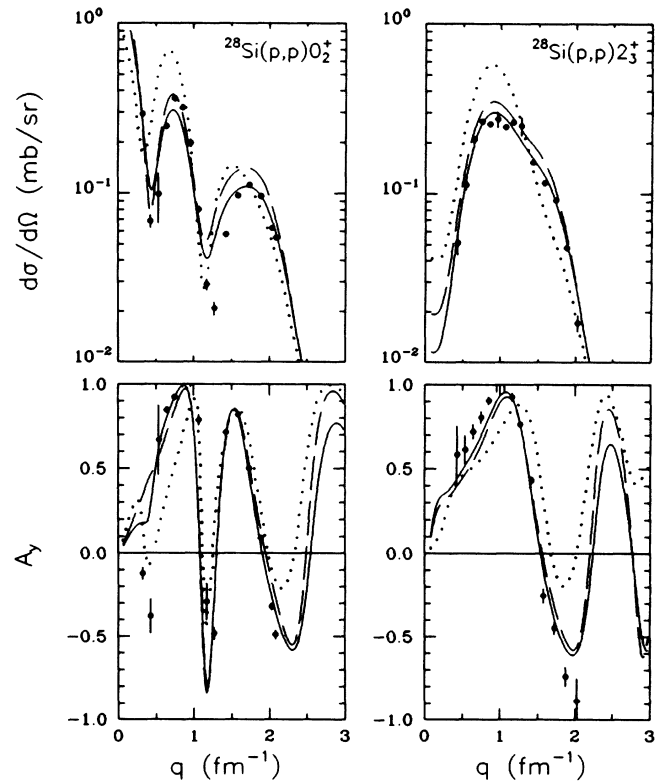
FIG. 6. Calculations are compared with data for the 0_2^+ and 2_3^+ states of ^{28}Si, which have "interior" densities. Dotted curves show IA calculations and dashed curves show LDA calculations based upon the PH interaction. The solid curves represent a fit of the effective interaction to ^{28}Si$(\vec{p}, p')$ data at 180 MeV.

present data and those from Schwandt *et al.*[4]

Strong density-dependent modifications of the effective interaction are required to accurately describe these data. Cross sections to the interior states, namely, 0_2^+ and 2_3^+, are suppressed by about a factor of 2 for $q < 1.2$ fm^{-1}. For larger q, the 2_3^+ cross section is significantly enhanced when Pauli blocking corrections are included in the LDA. Even the surface-peaked 2_1^+ and 4_1^+ states require substantial suppression of low-q cross sections. Similarly, the IA elastic cross section is too large for low q and too featureless for higher momentum transfer. Finally, we observe that the analyzing power for any state with significant interior strength displays considerably stronger negative oscillations than are predicted by the impulse approximation. These observations are consistent with the data for ^{16}O at both 180 and 135 MeV.[1,6] As described in Refs. 3, 6, and 21, these characteristics are explained by suppressed absorption and enhanced repulsion in the central component of the effective interaction.

The Pauli blocking corrections to the PH interaction provide a good qualitative description of these data. However, residual discrepancies are still significant. For example, the cross sections for both the 2_1^+ and 4_1^+ states remain above the data despite density dependent suppression. These discrepancies are similar to those observed in LDA calculations for similar surface-peaked states in ^{16}O, suggesting that modifications of the effective interaction need to be stronger at low density than predicted by the PH interaction.

An empirical effective interaction, producing the solid curves in Figs. 6 and 7, was fitted to these inelastic scattering data using the procedures described in Refs. 1 and 3. The PH interaction was used to produce the optical potential for the first iteration. Six parameters of the empirical effective interaction were fitted to cross section and analyzing power data for five states of ^{28}Si simultaneously. Additional uncertainties of $\pm 5\%$ for cross sections and ± 0.05 for analyzing powers were folded into the experimental uncertainties in order to regulate the relative weights assigned to the data. The fitted interaction was then used to produce a new optical potential and the fit was repeated. Approximately five iterations of this procedure were required for the interaction to converge and self-consistency between elastic and inelastic scattering to be achieved.
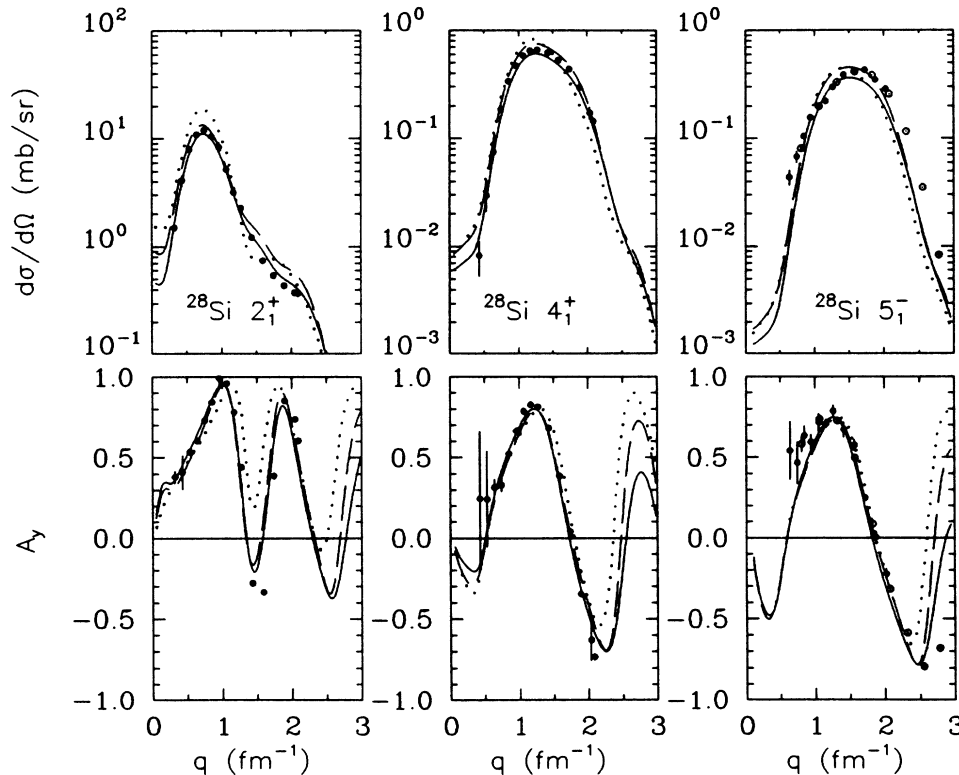
FIG. 7. Calculations are compared with data for the 2_1^+ and 4_1^+ and 5_1^- states of ^{28}Si, which have "surface" densities. Dotted curves show IA calculations and dashed curves show LDA calculations based upon the PH interaction. The solid curves represent a fit of the effective interaction to ^{28}Si$(\vec{p},p')$ data at 180 MeV. The solid points show our data and the open circles show the 5_1^- data of Olmer *et al.* (Ref. 5).

Significant improvements are achieved for all states but the 5_1^-. Most notably, the empirical interaction provides a much better description of the 2_1^+ cross section for large q, but is slightly too low at the peaks of both the 2_1^+ and 4_1^+ angular distributions. The shape of the 0_2^+ cross section is also much improved. In addition, the elastic scattering predicted by the empirical effective interaction is compared with the data in Fig. 8. Although these data were not included in the analysis, significant improvements are obtained in the analyzing power and in the cross section for momentum transfers outside the range $1.0 < q < 1.5$ fm^{-1}. Therefore, except for the 5_1^- cross section, the quality of the fit is quite good considering that data for many different states were analyzed simultaneously.
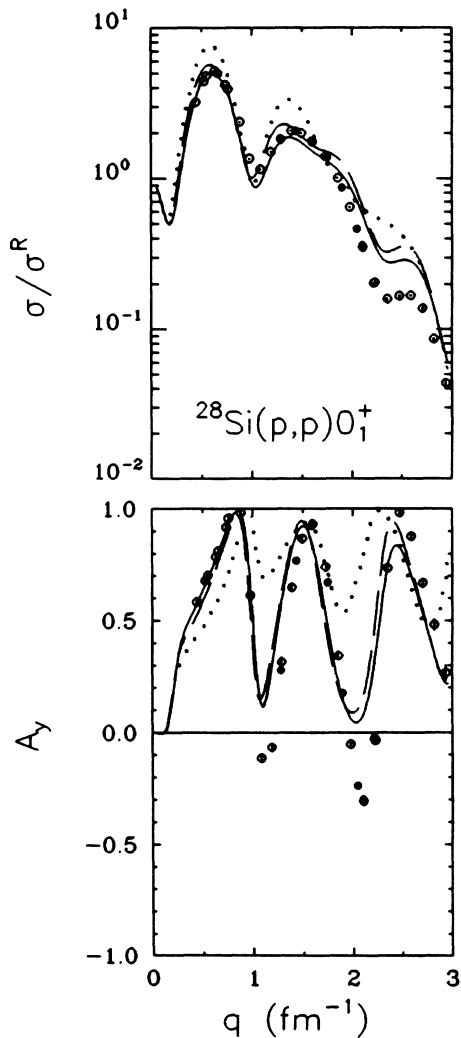
FIG. 8. Elastic scattering data from our experiment are shown as solid circles and the data of Schwandt et al. (Ref. 4) as open circles. An IA calculation is shown by dotted curves, an LDA calculation based upon the PH interaction by dashed curves, and the prediction of the empirical effective interaction fitted to inelastic scattering data for ^{28}Si by solid curves. Elastic cross sections are presented as ratios to Rutherford (σ_R) to enhance detail.

B. Other states of ^{28}Si

Similar calculations are shown in Figs. 9 and 10 for other normal-parity states of ^{28}Si which were not included in the analysis of the effective interaction. The electroexcitation data for these states is generally too limited to ensure that the transition densities are determined with enough accuracy to interpret the proton scattering data with confidence. Nevertheless, the analyzing powers are all predicted fairly accurately using the empirical effective interaction. For simple matter transitions of this type, the analyzing power is more sensitive to the interaction than it is to details of structure. In fact, all of the analyzing powers would have been the same in the absence of distortion. The differential cross section, on the other hand, is proportional to the square of the form factor and is thus more vulnerable to uncertainties in nuclear structure. We find that the cross-section data is described very well for the 2_4^+ state and moderately well for the 2_5^+ state. The larger discrepancies for the 1_1^- and 2_2^+ states probably indicate that these transition densities are inaccurate. The accuracy of the analyzing power calculations for these states suggests that multistep contributions are not likely to be the problem.

These results illustrate the importance of accurate form factor data. Ideally, electroexcitation data need to span at least the range $0 < q < 2.7$ fm^{-1}, within which the
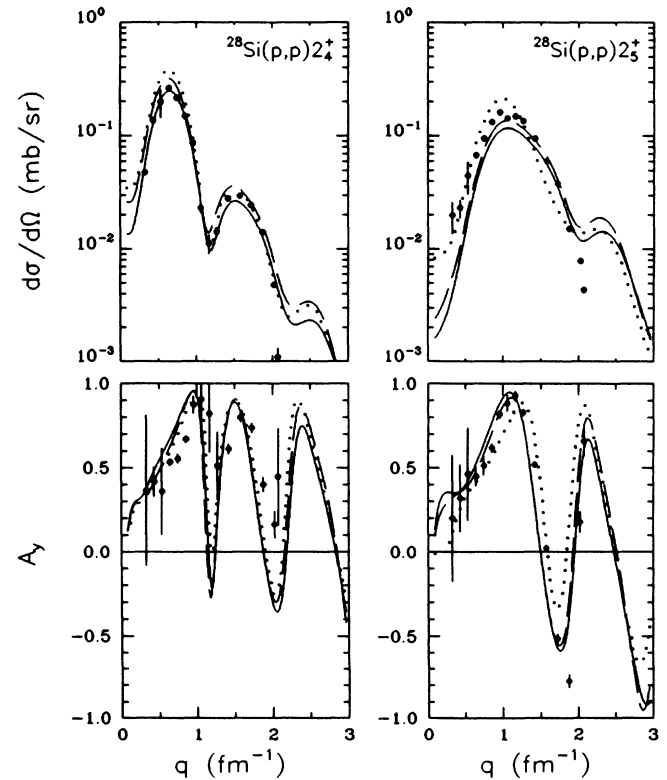
FIG. 9. Calculations using the empirical effective interaction are compared with data for the 2_4^+ and 2_5^+ states of ^{28}Si. Note that these data were excluded from the fit. See Fig. 6 for legend.

wave functions may contain large Fourier components, in order that transition densities may be determined with precision adequate to the needs of other reactions. For the present work, the small range covered by electron scattering data for some of the states is probably the most serious limitation upon the accuracy of the analysis. For example, the 5_1^- data displayed in Fig. 4 do not exclude the possibility that the form factor may be somewhat broader in q space than the present fit. A broader form factor would allow the proton scattering data in Fig. 7 to be fitted more accurately.

Ambiguities in the transition densities fitted to a limited range of momentum transfer can be especially severe when a node is present. In these cases, the form factor depends sensitively upon cancellations between interior and exterior contributions. Even worse, distortion alters the balance between these contributions to proton scattering. For the present application we note that the (e,e') data for the 0_2^+ state do not extend to low enough momentum transfer to clearly define the first peak of the form factor. Fortunately, however, the data near 1 fm^{-1} appears to be sufficiently precise to define the density with enough accuracy for use in the (p,p') analysis. The residual errors in the (p,p') fit for this state may well be due simply to inaccuracies in its form factor.

Similarly, the 1_1^-, 2_2^+, and 2_4^+ factors are not determined by the (e,e') data with enough accuracy to inter-

pret the (p,p') data with confidence. It is then no surprise that the (p,p') calculations for the 1_1^- and 2_2^+ states fail badly. In fact, the relatively good agreement obtained for the 2_4^+ data must be regarded as a pleasant surprise. Evidently, an accurate transition density was obtained for this state quite fortuitously. Finally, the (p,p') data for the 2_5^+ state suggest that the secondary maximum in its fitted form factor is spurious.

C. Consistency with ^{16}O

The empirical effective interaction proposed by Refs. 1 and 3 has the form

$$\mathrm{Re}t_{00}^C(q,\kappa_F)=S_1\mathrm{Re}t_{00}^C(q,0)$$

$$+\kappa_F^3 b_1\left[1+\left[\frac{q}{\mu_1}\right]^2\right]^{-1}, \tag{11a}$$

$$\mathrm{Im}t_{00}^C(q,\kappa_F)=(S_2-b_2\kappa_F^2)\mathrm{Im}t_{00}^C(q,0), \tag{11b}$$

$$\mathrm{Re}\tau_0^{LS}(q,\kappa_F)=S_3\mathrm{Re}\tau_0^{LS}(q,0)$$

$$+\kappa_F^3 b_3\left[1+\left[\frac{q}{\mu_3}\right]^2\right]^{-2}, \tag{11c}$$

where $\kappa_F=k_F/1.33$ describes the local Fermi momentum relative to saturation. The ranges were chosen as $\mu_1=1.5$
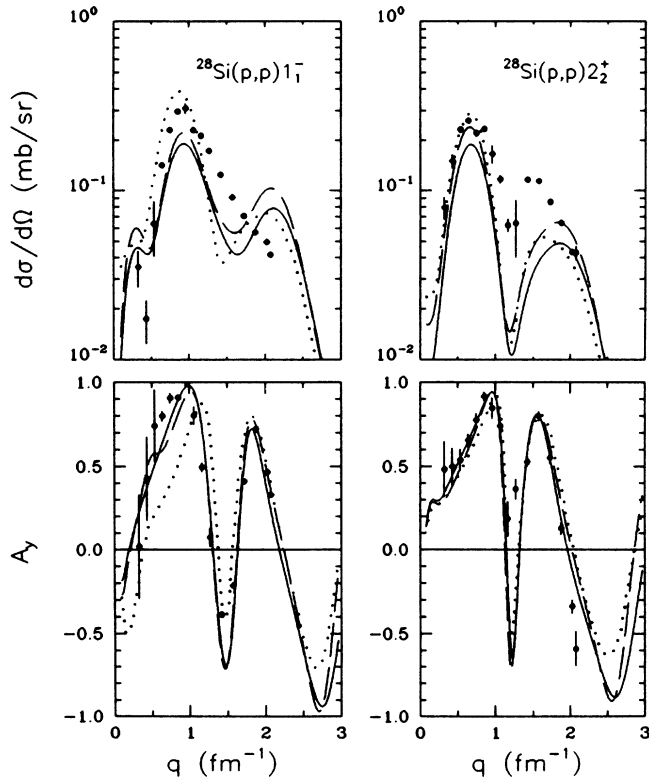
FIG. 10. Calculations using the empirical effective interaction are compared with data for the 1_1^- and 2_2^+ states of ^{28}Si. Note that these data were excluded from the fit. See Fig. 6 for legend.
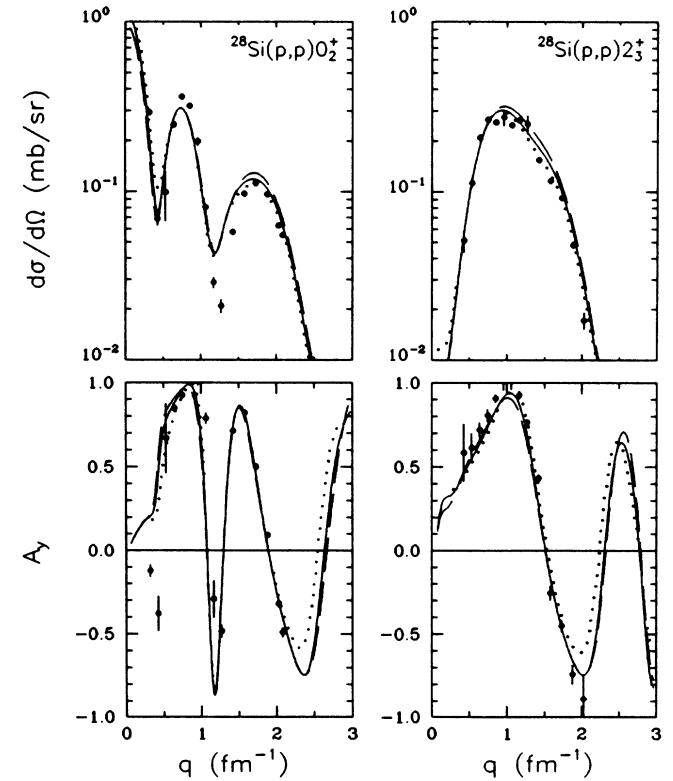
FIG. 11. Data for the 0_2^+ and 2_3^+ states of ^{28}Si are compared with calculations based upon empirical effective interactions fitted to the ^{28}Si data alone (dotted curves), the ^{16}O data alone (dashed curves), or the combined ^{16}O+^{28}Si data set (solid curves).

TABLE II. Empirical effective interactions for 180 MeV nucleons.

Data set	S_1	b_1 (MeV fm^3)	S_2	b_2	S_3	b_3 (MeV fm^3)
^{16}O	0.749	62.9	0.764	0.228	0.883	0.51
^{28}Si	0.792	69.5	0.786	0.113	0.860	-1.32
^{16}O$+^{28}$Si	0.787	71.5	0.806	0.180	0.860	0.61

fm^{-1} and $\mu_3 = 6.0$ fm^{-1}. The scale factors S_i permit modification of the interaction at low density. The b_1 parameter describes a repulsive core in Ret^c that is proportional to density. The b_2 parameter describes Pauli blocking of absorption and is expected to exhibit an E^{-1} energy dependence.[22] The b_3 parameter describes a repulsive core in the spin-orbit interaction and is expected to be small and nearly independent of energy.[2] Finally, the Imτ^{LS} contribution is rather small and was taken from the PH theory.[2]

The parameters of the empirical effective interaction fitted to data for ^{28}Si are compared in Table II with those fitted in Ref. 1 to data for ^{16}O. Both analyses agree that the effective interaction in finite nuclei needs to be substantially suppressed at low density and that the subsequent density dependence is somewhat weaker than predicted by the PH theory for infinite nuclear matter.

However, the Pauli damping factor, namely, the b_2 parameter for Imt_{00}^c, fitted to ^{28}Si data is only half that which emerged from the ^{16}O analysis. Although this difference might suggest A dependence in the effective interaction for finite nuclei, some care in the interpretation of parameter ambiguities must be exercised before such a conclusion can be supported.

To investigate the compatibility of the two analyses, we performed a third fit using both data sets simultaneously, including five states of ^{16}O and five states of ^{28}Si in a global fit. The fit was iterated until self-consistency was again achieved in the manner described above. The result, also listed in Table II, is intermediate between the two independent results. In particular, the b_2 parameter fitted to the combined data is near the average of the previous values. The scale factors are almost unaffected and b_3 is nearer the ^{16}O result. Nevertheless, the quality of
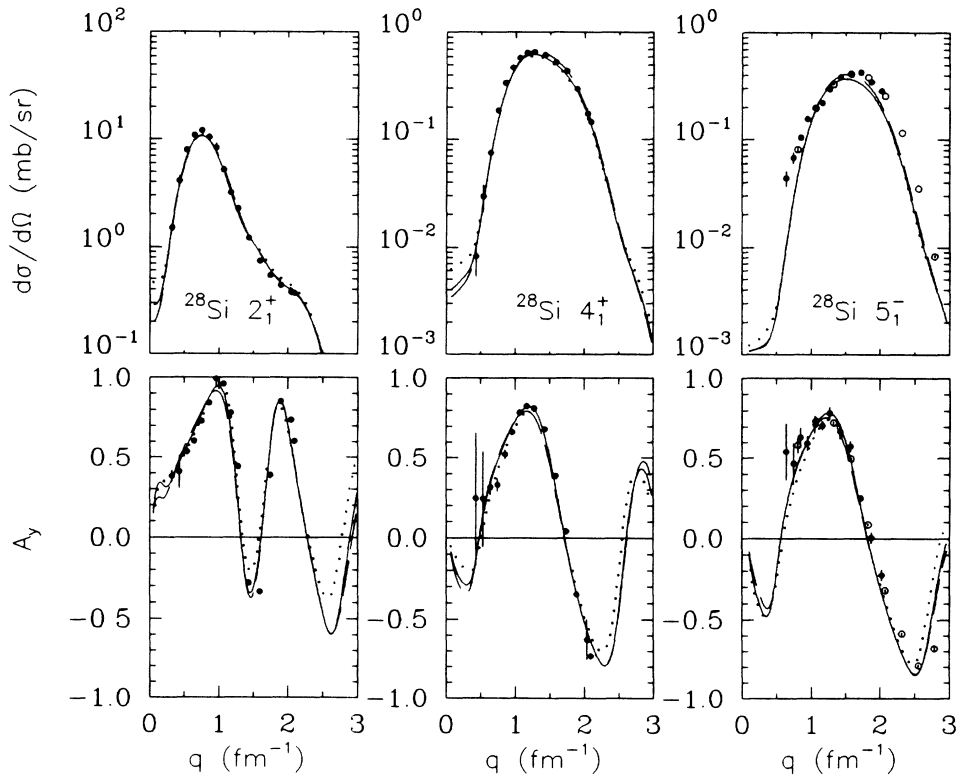
FIG. 12. Data for the 2_1^+ and 4_1^+ and 5_1^- states of ^{28}Si are compared with calculations based upon empirical effective interactions fitted to the ^{28}Si data alone (dotted curves), the ^{16}O data alone (dashed curves), or the combined ^{16}O$+^{28}$Si data set (solid curves).
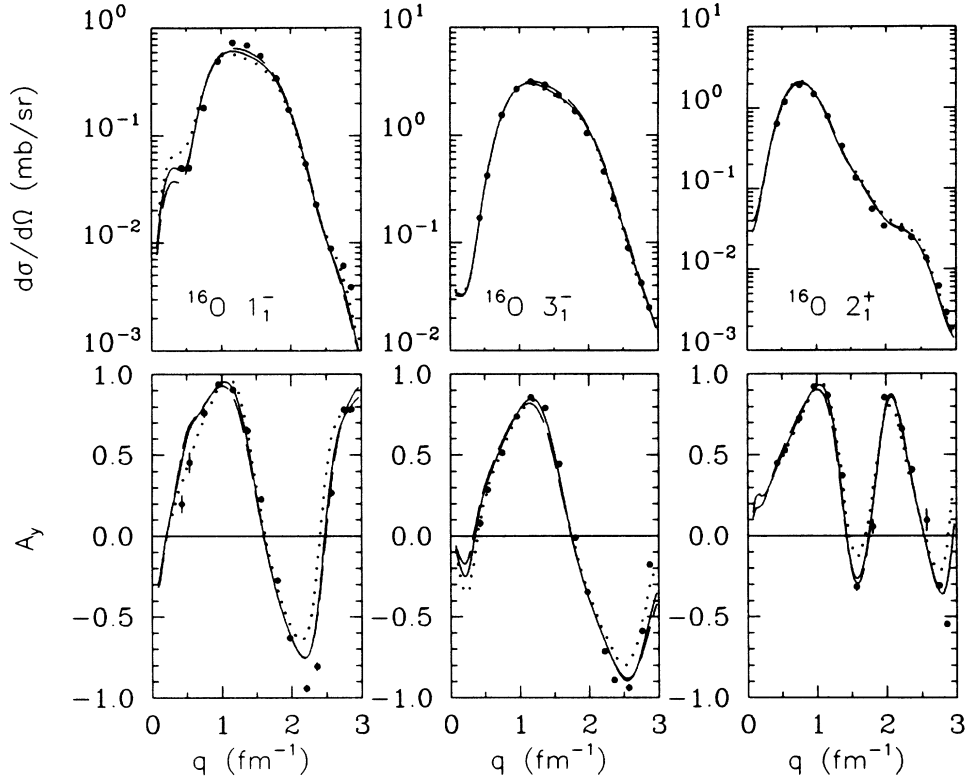
FIG. 13. Data for selected states of ^{16}O are compared with calculations based upon empirical effective interactions fitted to the ^{28}Si data alone (dotted curves), the ^{16}O data alone (dashed curves), or the combined ^{16}O + ^{28}Si data set (solid curves).

the fits is hardly affected by these changes.

Elastic and selected inelastic scattering calculations based on all three empirical interactions are compared in Figs. 11–14. The differences are always rather small and are often almost indiscernible. Generally, the ^{16}O analysis and the combined analysis are slightly superior to the results obtained by fitting only the ^{28}Si data. There are several reasons for this. First, the range of momentum transfer spanned by the ^{28}Si data is somewhat too small to discriminate well between various contributions to the effective interaction. Second, the electron scattering data for ^{28}Si is rather sparse for the 0_2^+ and 2_3^+ states. The 5_1^- data are also somewhat limited in momentum transfer. Hence, transition densities are known less accurately for ^{28}Si than for ^{16}O. Finally, although the reason is unclear, the fit to the 5_1^- cross section is rather poor. Thus, although the fit to the ^{28}Si data alone is compatible with the ^{16}O data and is superior to the PH theory, the analyses based upon the full data set or upon the ^{16}O data alone are probably more reliable and produce interactions that are in better agreement.

Therefore, we conclude that there is no compelling evidence for A dependence in the effective interaction. Nevertheless, the effective interaction for finite nuclei clearly differs from the interaction for infinite nuclear matter in two important respects. First, the interaction for low densities is substantially reduced with respect to expectations based upon the local density approximation. Second, the density dependence is weaker than predicted by nuclear matter theory. Essentially the same results
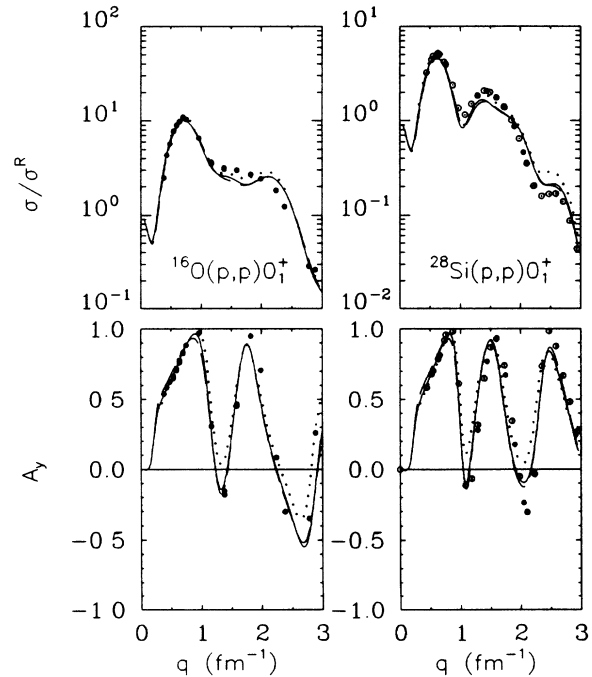
FIG. 14. Data for elastic scattering are compared with calculations based upon empirical effective interactions fitted to the ^{28}Si data alone (dotted curves), the ^{16}O data alone (dashed curves), or the combined ^{16}O + ^{28}Si data set (solid curves).

are obtained for ^{16}O and ^{28}Si at 180 MeV and for ^{16}O at 135 MeV. Thus, although the quantitative results depend in some degree upon ambiguous choices of free interaction and technique, the qualitative features are unambiguous.

V. CONCLUSIONS

We have developed a parametrization of medium modifications to the two-nucleon effective interaction guided by the results of nuclear matter calculations. This parametrization is capable of accurately describing any of the theoretical interactions presently available. Although these calculations predict qualitatively similar density dependences, their quantitative predictions differ so much that the applicability of the local density approximation to finite systems cannot be established using only *ab initio* calculations. Therefore, we have developed a guided phenomenology which fits empirical medium modifications to inelastic scattering data and thereby tests the LDA in a manner largely independent of the accuracy of nuclear matter calculations.

If the LDA is to be considered sound, the empirical effective interaction must satisfy three basic criteria. First, a unique effective interaction must be capable of describing all relevant data for a given target and energy. Second, the effective interaction should be independent of target. Third, the parameters should vary smoothly with energy and hopefully be similar to theoretical predictions.

Our previous work on ^{16}O at 135 and 180 MeV satisfied the first and third criteria. The present work supports the second criterion by showing that the effective interaction for ^{28}Si is consistent with the ^{16}O results. Therefore, the LDA seems to provide an accurate model for the density dependence of the effective interaction in nuclei.

The empirical effective interaction for normal-parity isoscalar transitions in the energy range $E_p = 100$–200 MeV exhibits two major differences from theoretical interactions. First, the interaction for low density is suppressed much more strongly than predicted by the local density approximation. Second, the density dependence for higher densities is substantially weaker than predicted by the PH theory, which is the most accurate of the three available calculations for this type of transition. Although the quantitative results depend upon choices of free interaction and analysis procedure, these qualitative results are independent of such choices. We consider these properties of the effective interaction in finite nuclei to be well established. Further progress awaits the development of practical theories of the effective interaction in finite nuclei.

[1] J. J. Kelly, J. M. Finn, W. Bertozzi, T. N. Buti, F. W. Hersman, C. Hyde-Wright, M. V. Hynes, M. A. Kovash, B. Murdock, P. Ulmer, A. D. Bacher, G. T. Emery, C. C. Foster, W. P. Jones, D. W. Miller, and B. L. Berman, Phys. Rev. C **41**, 2504 (1990).

[2] H. V. von Geramb, in *The Interaction Between Medium Energy Nucleons in Nuclei—1982*, AIP Conf. Proc. No. 97, edited by H. O. Meyer (AIP, New York, 1983), p. 44; L. Rikus, K. Nakano, and H. V. von Geramb, Nucl. Phys. **A414**, 413 (1984).

[3] J. J. Kelly, Phys. Rev. C **39**, 2120 (1989).

[4] P. Schwandt, H. O. Meyer, W. W. Jacobs, A. D. Bacher, S. E. Vigdor, M. D. Kaitchuck, and T. R. Donoghue, Phys. Rev. C **26**, 55 (1982).

[5] C. Olmer, A. D. Bacher, G. T. Emery, W. P. Jones, D. W. Miller, H. Nann, P. Schwandt, S. Yen, T. E. Drake, and R. J. Sobie, Phys. Rev. C **29**, 361 (1984).

[6] J. J. Kelly, W. Bertozzi, T. N. Buti, J. M. Finn, F. W. Hersman, C. Hyde-Wright, M. V. Hynes, M. A. Kovash, B. Murdock, B. E. Norum, B. Pugh, F. N. Rad, A. D. Bacher, G. T. Emery, C. C. Foster, W. P. Jones, D. W. Miller, B. L. Berman, W. G. Love, J. A. Carr, and F. Petrovich, Phys. Rev. C **39**, 1222 (1989).

[7] T. N. Buti, J. Kelly, W. Bertozzi, J. M. Finn, F. W. Hersman, C. Hyde-Wright, M. V. Hynes, M. A. Kovash, S. Kowalski, R. W. Lourie, B. Murdock, B. E. Norum, B. Pugh, C. P. Sargent, W. Turchinetz, and B. L. Berman, Phys. Rev. C **33**, 755 (1986).

[8] P. M. Endt and C. van der Leun, Nucl. Phys. **A310**, 1 (1978).

[9] Q. Chen, Ph.D. thesis, Indiana University, 1988.

[10] See AIP document No. PAPS PRVCA-41-2514-14 for 14 pages containing a complete tabulation of the data described in this paper. Order by PAPS number and journal references from American Institute of Physics, Physics Auxiliary Publication Service, 335 E. 45th Street, New York, NY 10017. The price is $1.50 for each microfiche or $5.00 for photocopies. Airmail additional. Make checks payable to the American Institute of Physics.

[11] T. de Forest and J. D. Walecka, Adv. Phys. **15**, 1 (1966).

[12] C. E. Hyde-Wright, Ph.D. thesis, MIT, 1984.

[13] P. M. Endt, At. Data Nucl. Data Tables **23**, 3 (1979).

[14] G. Mülhaupt, Ph.D. thesis, Johannes Gutenberg Universität zu Mainz, 1970.

[15] S. Yen, Ph.D. thesis, University of Toronto, 1983, and private communication.

[16] S. Yen, R. J. Sobie, T. E. Drake, H. Zarek, C. F. Williamson, S. Kowalski, and C. P. Sargent, Phys. Rev. C **27**, 1939 (1983).

[17] G. C. Li, M. R. Yearian, and I. Sick, Phys. Rev. C **9**, 1861 (1974); I. Sick, private communication.

[18] S. W. Brain, A. Johnston, W. A. Gillespie, E. W. Lees, and R. P. Singhal, J. Phys. G **3**, 821 (1977).

[19] K. E. Whitner, C. F. Williamson, B. E. Norum, and S. Kowalski, Phys. Rev. **22**, 374 (1980).

[20] H. de Vries, C. W. de Jager, and C. de Vries, At. Data Nucl. Data Tables **36**, 495 (1987).

[21] J. Kelly, W. Bertozzi, T. N. Buti, F. W. Hersman, C. Hyde, M. V. Hynes, B. Norum, F. N. Rad, A. D. Bacher, G. T. Emergy, C. C. Foster, W. P. Jones, D. W. Miller, B. L. Berman, W. G. Love, and F. Petrovich, Phys. Rev. Lett. **45**, 2012 (1980).

[22] E. Clementel and C. Villi, Nuovo Cimento **2**, 176 (1955).